Journal of
Manufacturing and Materials Processing

MDPI

Article

Determination of the Cutting-Edge Microgeometry Based on Process Forces during Peripheral Milling of Ti-6Al-4V Using Machine Learning

Matthias Wimmer *, Roman Hartl and Michael F. Zaeh

TUM School of Engineering and Design, Technical University of Munich, 85748 Garching, Germany
* Correspondence: matthias.wimmer@iwb.tum.de

Abstract: The residual stress state of the machined sub-surface influences the service quality indicators of a component, such as fatigue life, tribological properties, and distortion. During machining, the radius of the cutting edge changes due to tool wear. The cutting-edge rounding significantly affects the residual stress state in the part and the occurring process forces. This paper presents a tool wear prediction model based on in-process measured cutting forces. The effects of the cutting-edge geometry on the force behavior and the machining-induced residual stresses were examined experimentally. The resulting database was used to realize a Machine Learning algorithm to calculate the hidden value of tool wear. The predictions were validated by milling experiments using rounded cutting edges for different process parameters. The microgeometry of the cutting edge could be determined with a Root Mean Square Error of 8.94 µm.

Keywords: milling; titanium alloy Ti-6Al-4V; residual stresses; process forces; cutting-edge radius; machine learning; tool wear prediction; supervised learning; multilayer perceptron

Citation: Wimmer, M.; Hartl, R.; Zaeh, M.F. Determination of the Cutting-Edge Microgeometry Based on Process Forces during Peripheral Milling of Ti-6Al-4V Using Machine Learning. *J. Manuf. Mater. Process.* **2023**, *7*, 100. https://doi.org/10.3390/jmmp7030100

Academic Editor: Mohamed Elbestawi

Received: 6 April 2023
Revised: 8 May 2023
Accepted: 17 May 2023
Published: 19 May 2023

1. Introduction

The titanium alloy Ti-6Al-4V is widely used in the aerospace and medical industries due to its advantageous material properties. These include an excellent strength-to-weight ratio, corrosion resistance and low thermal conductivity [1]. These properties also present challenges in the manufacturing process, where machining is often used to produce the components. Titanium and its alloys are among the most difficult materials to machine [2]. The mechanical and chemical properties of Ti-6Al-4V result in high cutting forces and heat generation, causing excessive tool wear of the cutting edges [2]. In addition, the integrity of the surface of the machined components is altered by the machining process. In order to ensure the quality, functionality, and durability of the finished part, this is one of the most critical factors. In this respect, an important area of finishing machining is the improvement in the functional performance of high-value components [1,3,4].

In particular, the thermo-mechanical load applied by machining alters the residual stress state of the sub-surface [5]. Residual stress represents the remaining stress in the machined material after the external load has been removed, reflecting the total macro-stresses in the machined sub-surface zone. The residual stress state significantly affects the performance of the component such as corrosion resistance and fatigue life [6]. The change in residual stresses can therefore be used to assess the overall structural strength of the component and its propensity to fatigue failure in service [7]. Mechanical loads tend to cause compressive stresses, while thermal effects generally cause residual stresses in the tensile range [8,9]. Compressive residual stresses have been found to positively affect the fatigue life, creep behavior and crack propagation resistance, while tensile residual stresses are usually detrimental [1,10]. The amount of residual stress change is defined by the stress and heat sources that affect the sub-surface during the machining process. These can be

characterized by examining the primary shear zone and the tool-workpiece interface, and are significantly dependent on the microgeometry of the cutting edge [8].

2. Influence of the Cutting-Edge Radius

2.1. Residual Stresses

In machining with a geometrically defined cutting edge, the main contact area between the tool and the workpiece is formed by cutting-edge rounding. Consequently, the cutting process is significantly influenced by the micro-geometry of the cutting edge [11,12]. The geometry of the cutting edge is a significant factor in influencing the tool–workpiece–chip contact, the occurring thermo-mechanical loads in the contact area, and the residual stresses induced by machining [5,13]. Therefore, the influence of rounded cutting edges on the resulting surface integrity has been evaluated for different materials and processes in the literature. To investigate the impact of the edge radius on the machining-induced residual stresses, Denkena et al. performed turning experiments on AISI 52100 [11]. They found that larger-edge radii caused higher compressive residual stresses and the affected surface layer increased. Changing the cutting-edge radius from 40 µm to 105 µm, the authors measured an increase in the maximum compressive stresses for both the circumferential and axial stress directions from 570 MPa to 1050 MPa. As a result of adopting a larger cutting-edge rounding, they witnessed higher passive forces, which led to an increase in the mechanical load and consequently to more plastic deformation in the sub-surface. The effect of the cutting-edge radius on the surface and near-surface residual stresses in up- and down-milling was examined by Wyen et al. using a one-fluted milling tool [14]. In this study, the titanium alloy Ti-6Al-4V was machined. Measurements of the residual stresses after machining showed an increase in maximum compressive stress on the surface due to the change in the cutting-edge radius from 310 MPa using a cutting-edge rounding of 6 µm to 600 MPa with a radius of 50 µm, whereas no uniform trend was observed for down-milling.

Furthermore, the surface compressive residual stress increased, but the depth of the maximum compressive stress d_{RS} (Figure 1d) and the range of influence of the machining-induced residual stress decreased as the edge radius changed from 0.01 mm to 0.03 mm. Tools with sharp and rounded cutting edges were used by Coelho et al. and Li et al. [12,15]. After turning Inconel 718 and milling AISI H13 steel, both identified the generation of compressive residual stresses independently of the process. Higher machining-induced compressive stresses were induced with rounded cutting edges rather than with sharp tools. Nespor compared the influence of the edge geometry on residual stresses after machining Ti-6Al-4V using ball end milling and orthogonal turning and planing [13]. The surface residual stresses in the cutting direction increased with a larger edge radius for all performed machining processes, and the absolute values were higher for turning than for planing. Ozel and Ulutan compared the effect of the cutting-edge radius on the resulting residual stress profiles for turning of Ti-6Al-4V [16]. In the radial direction, all experiments induced compressive residual stresses both on the surface and at the sub-surface of the material. However, in the circumferential direction, tensile residual stresses on the machined surface were measured, which gradually became compressive in the depth direction. Wyen and Wegener confirmed that the increased thermal and mechanical loads due to higher cutting-edge radii result in an increase in the process forces that act directly on the surface during machining [17]. Additional material deformation occurs at the front of the cutting edge due to its rounded shape, particularly where the cutting edge is in contact with the workpiece. The plastic deformation of the sub-surface (Figure 1d) led to compressive stresses in both up- and down-milling. The stresses are of different magnitudes depending on the direction. The compressive stresses in the cutting direction were smaller than those in the direction perpendicular to the cutting speed.

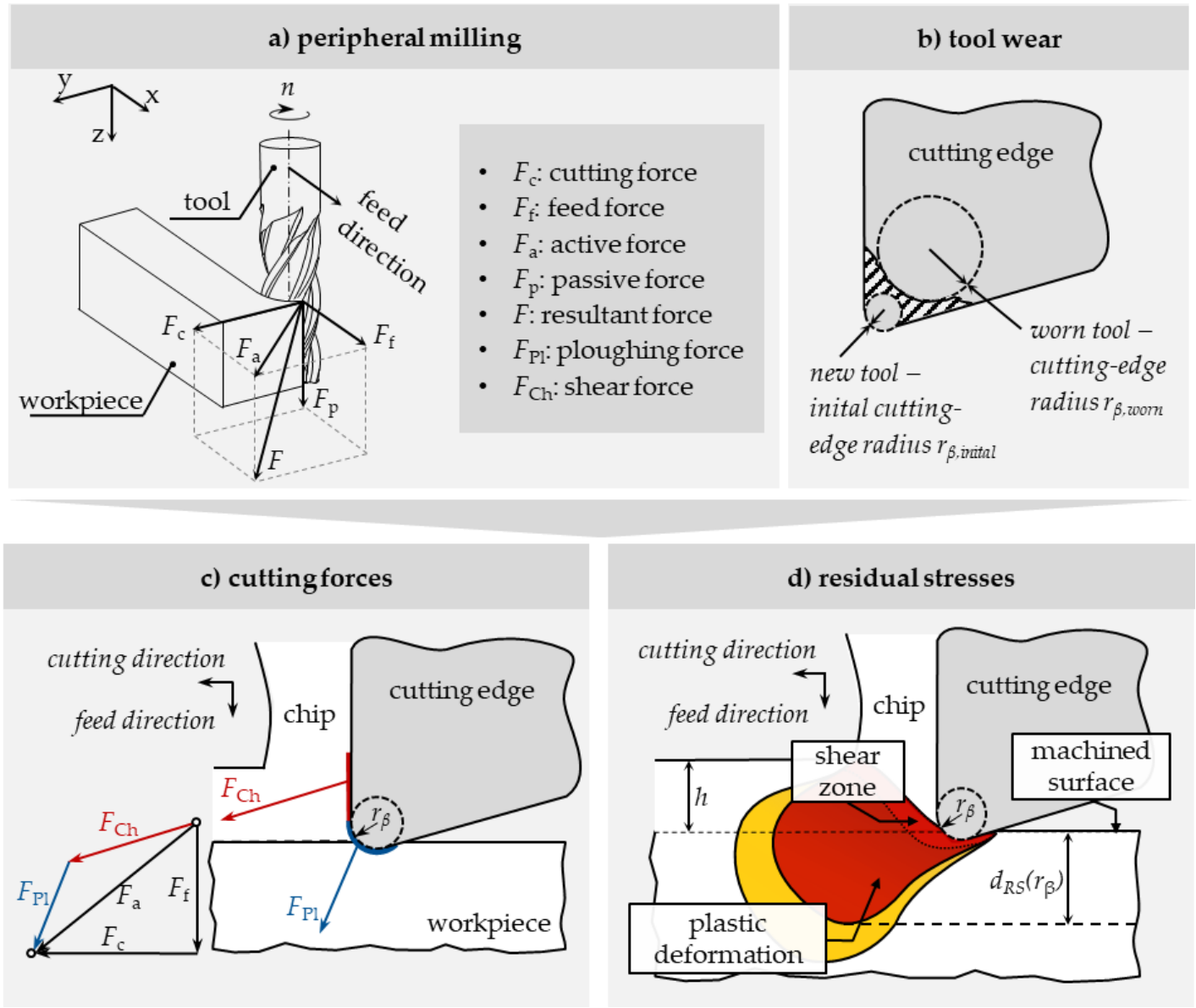

Figure 1. (**a**) Process forces in peripheral milling. (**b**) Change in the cutting-edge radius due to tool wear. (**c**) Ploughing forces due to the cutting-edge radius. (**d**) Influence of the cutting-edge rounding on plastic deformation according to Schoop et al., Albrecht, DIN 6580 and DIN 6584 [8,18–20].

2.2. Process Forces

Due to the tool-workpiece contact during the peripheral milling process, a resulting force F occurs. It comprises the cutting force F_c, the feed force F_f, and the passive force F_p (Figure 1a) [19]. In general, total forces recorded in a cutting process are the sum of individual forces acting on the tool flank face, its cutting edge, and the rake face [21]. The cutting edge is assumed to have an ideal sharp geometry in orthogonal cutting theory [22]. In practice, however, the cutting edge is rounded (Figure 1b), which causes a severe elastic and plastic deformation of the material around the cutting edge to occur simultaneously with the cutting process. This mechanism is referred to as the ploughing effect and can be described in terms of the ploughing force F_{Pl} (Figure 1c) acting directly on the cutting edge [18]. The percentage of this force in the total cutting force has often been considered insignificant in the previous literature and sometimes been neglected in force modeling for simplification reasons. A cutting force prediction model that considers the edge geometry was proposed in 1960 by Albrecht [18]. On the basis of this early model, Moufki et al.

pointed out that the importance of the ploughing force depends on the relation between the uncut chip thickness h and the cutting-edge rounding r_β [23]. The ploughing force can dominate when the uncut chip thickness is comparable to the cutting-edge radius. The rounded cutting edges influence the active force components including the ploughing forces and tool face friction, which are especially important in machining titanium alloys such as Ti-6Al-4V. Wegener and Wyen investigated the effect of different cutting-edge radii on the cutting and feed forces during the orthogonal turning of Ti-6Al-4V [14,17]. The force components increased with the increasing cutting-edge radius where the cutting force was less sensitive than the feed force. Experiments conducted during milling of SUS-316L steel by Lv et al. showed that a change in the cutting-edge radius from 4 to 15 µm led to an increase of 23% in the cutting force and 56% in the feed force for an uncut chip thickness h of 0.2 mm [24].

The radius of the cutting edge significantly influences the occurring cutting forces and therefore the mechanical load on the workpiece during milling. Particularly for titanium, which is used in applications requiring high mechanical integrity, information on the dependence of the surface integrity on the cutting-edge geometry is essential. The cutting-edge radius changes during milling as a result of tool wear (Figure 1b). In order to be able to determine the resulting residual stress state, a prediction of the microgeometry of the cutting edge is required. Therefore, the aim of this paper is to predict the cutting-edge radius. None of the currently available analytical, numerical, or empirical wear monitoring methods is sufficient to determine a nominal cutting-edge rounding value during milling.

For this reason, a new approach in artificial intelligence is presented, which uses the relationships between the process parameters, the cutting-edge radius and the measured cutting forces. In particular, machine learning (ML) algorithms can reveal the unknown underlying structure in the data and are therefore applied. To obtain the tool wear prediction model, experiments were first performed to generate a data set, including

- the measured process forces,
- the process parameters, and
- the measured cutting-edge radius.

The measured data and the process parameters were used as input and output values for the ML method. Characteristic values, such as the average forces, were extracted from the measured force signals through signal processing and data analysis. The cutting-edge radii were determined using a laser scanning microscope and extracted from the obtained profile. Because the objective is the determination of the cutting-edge rounding, the pre-processed force data and process parameters are input values. The cutting-edge radius for each data sample is assigned to the output value. This provides labeled data that define the problem at hand as a problem in the supervised learning setup. Furthermore, because the goal is to determine a nominal value for the cutting-edge rounding, the problem is one of regression [25]. The multilayer perceptron (MLP) algorithm was used as a universal function approximator [25,26].

3. Experiments and Procedures

In order to evaluate the influence of the microgeometry of the cutting edge on the cutting forces during peripheral milling of Ti-6Al-4V, down-milling experiments were conducted on a GROB G352-T 5-axis machining center. The geometry of the plates as samples was 100 mm × 100 mm × 10 mm. A constant cutting speed v_c of 30 m/min and a radial depth of cut a_e of 0.5 mm were used. The workpiece thickness of 10 mm was equal to the axial depth of cut. The machining parameters corresponded to those typically used for machining titanium. The end mills were OptiMill®-Titan-HPC SCM39 uncoated solid carbide milling tools with a diameter of 12 mm and four teeth with a helix angle β of 40° from MAPAL Dr. Kress KG. According to the manufacturer's specification regarding the cutting edges, the rake angle γ was 5.0 ± 0.13° and the clearance angle α_c was 11.4 ± 0.12°. In addition, no cutting fluids were applied, thus eliminating them as a possible factor influencing the process forces.

3.1. Force Measurement

During the peripheral milling experiments, a tool holder with integrated sensors was used to measure the forces [27]. The occurring forces generated a bending moment in the tool holder, which can be converted into the cutting forces in the Cartesian coordinate system, F_x, F_y, and F_z. Using strain gauges arranged at an angle of 90° to each other, the force components in the x-, y- and z-directions were measured [28]. Data acquisition was performed with a sampling rate of 2 kHz and the recorded forces were transmitted to the data receiver via Wi-Fi. The experimental setup is illustrated in Figure 2.

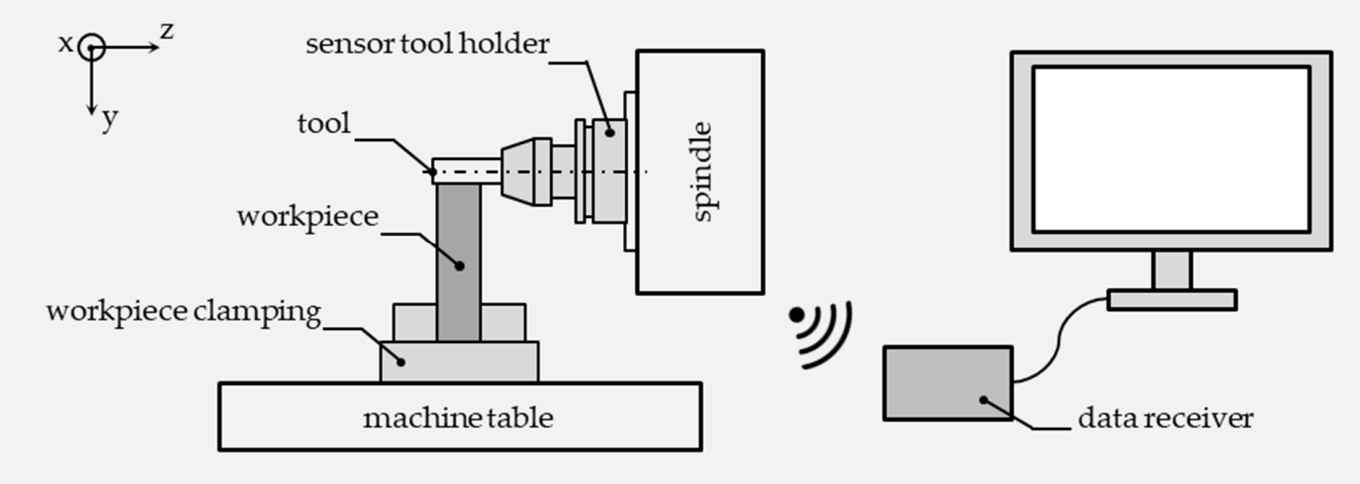

Figure 2. Experimental setup.

3.2. Process Parameters

The process parameters used for the experiments are given in Table 1. A constant depth of cut a_e of 0.5 mm was selected because the investigations focus on the finishing process (a_e between 0.1 and 0.5 mm). In order to reduce thermal effects leading to an increase in tool wear, a low cutting speed v_c of 30 m/min was used for the peripheral milling of Ti-6Al-4V. The first set of experiments involved nine tools (No. 1–9) with new cutting edges. To ensure repeatability, three tools were used, each with the same feed per tooth f_z. Tool wear tests were performed until each initially sharp tool had reached a milling length of 35.0 m. This limit was set because wear marks appeared on the tool as well as visible bumps on the component surface at this distance. Therefore, to obtain a reasonable data set size, the measurement intervals were chosen in steps of 0.5 m. A total of 630 samples was generated.

Table 1. Process parameters.

No.	Tool	a_e in mm	v_c in m/min	f_z in mm	r_β in µm
1	1/2/3	0.5	30	0.04	variable
2	4/5/6	0.5	30	0.06	variable
3	7/8/9	0.5	30	0.08	variable

3.3. Measurement of the Cutting-Edge Radius

The cutting edge is defined by the DIN 6581 standard [28]. It is the part of the tool that effectively produces the surface of the component. While the characterization of the macrogeometry of the cutting edge is internationally standardized [28,29], there is no standard method for describing the microgeometry of the cutting edge, which is the actual shape of the intersection of the flank and the rake face of a tool [30]. The cutting-edge rounding was formed by an approximating circle. Extensive research on the characterization and measurement of the cutting-edge profile has been performed by Wyen [30].

The method developed is shown in Figure 3, which was used for the measurement of the radius of the cutting edge. The procedure can be divided into five individual steps, with the aim of determining a reference circle (dotted red circle in Figure 3) that is adapted to the contour of the microgeometry of the cutting edge. The resulting radius r_β of the circle corresponds to the radius of the rounded cutting edge. In the first step, a straight-line fitting is performed according to the least squares method on the flank and rake face. Using the determined straight lines, the bisector of the wedge angle β can be calculated, which intersects the cutting-edge profile at the point p_{int} (step 2). Based on the intersection point p_{int}, a circle can be inserted that is tangent to the two fitting lines. The new upper bound for the least squares fitting range results from the points where the circle contacts the straight fitting lines (step 3). By repeating steps 2 and 3, the iterative geometric fitting can minimize the difference between the points where the straight lines are tangent to the circle and the upper fitting limit of the previous step to approximately zero (step 4). This allows the determination of the absolute limit of the transition between the macro- and micro-geometry, which defines the area for the circle fitting to determine the cutting-edge radius r_β (step 5).

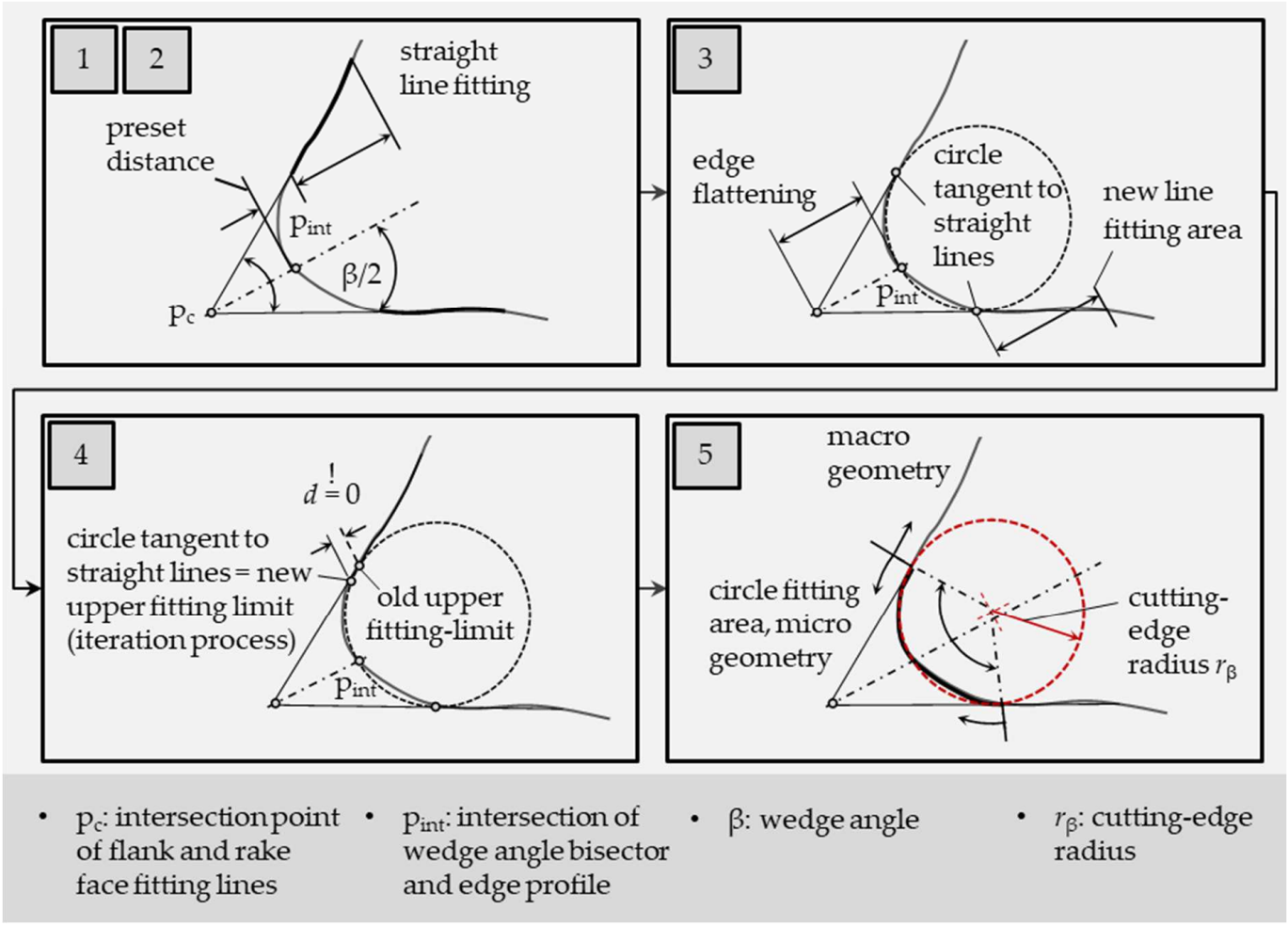

Figure 3. Method for measuring of the cutting-edge radius according to Wyen [30].

This approach drastically reduces the uncertainty of the point sensitivity and the deviations of a single point. After defined intervals of the milling length of 0.5 m, the cutting edges of the milling tool were measured. In order to determine the maximum cutting-edge rounding $r_{\beta,max}$ due to tool wear during the experiments described in Table 1, the tool was removed from the machine and placed in an ultrasonic bath to remove adhering chips. The microgeometry of the tools was measured using a KEYENCE VK-X1050 laser

scanning microscope. The height profile obtained by the microscope was analyzed using the MultiFile Analyzer software included in the VK-X1050.

3.4. Residual Stress Measurement

The individual cutting edges of the tool were prepared to create defined cutting-edge radii. The edges were symmetrically rounded by tool grinding using a CNC tool grinder. The radii were determined using the characterization method described in Section 3.2. For the second series of experiments (Table 2), eight different tools (No. 4–11) were prepared, with cutting edge radii ranging from 5 ± 1 µm (new tool) to 60 ± 1 µm. The cutting speed v_c and the radial depth of cut a_e were kept constant and the feed per tooth was varied from 0.04 to 0.08 mm in steps of 0.2 mm. The objective was to determine the quantitative relationship between the cutting-edge rounding and the machining-induced residual stresses on the machined surface.

Table 2. Experimental plan for residual stress measurements.

No.	a_e in mm	v_c in m/min	f_z in mm	r_β in µm
4	0.5	30	0.04, 0.06, 0.08	5 (sharp)
5	0.5	30	0.04, 0.06, 0.08	10
6	0.5	30	0.04, 0.06, 0.08	20
7	0.5	30	0.04, 0.06, 0.08	25
8	0.5	30	0.04, 0.06, 0.08	30
9	0.5	30	0.04, 0.06, 0.08	40
10	0.5	30	0.04, 0.06, 0.08	50
11	0.5	30	0.04, 0.06, 0.08	60

The residual stresses on the machined surface along and perpendicular to the feed direction were measured using X-ray diffraction (XRD). Three repetitions were performed in each case and the scatter was calculated. The measurement was performed using a Stresstech Xstress3000 XRD device with a G2R goniometer. The stresses were determined using the sin-2ψ method. This method is based on determining the elastic lattice strains, which are converted to stresses by the 3D form of Hooke's law [27,31]. The macro stresses distort the crystal lattice, resulting in an angular shift of the diffraction peak selected to measure the residual stresses. These measurements provide information on the residual stresses on the surface because the X-ray beam penetrates only to a depth of about 5 µm [32].

4. Experimental Results

4.1. Force Behavior

During the peripheral milling tests, the force signals in the Cartesian directions (F_x, F_y, and F_z) were recorded. Afterward, a filter was applied to reduce the impact of the noise on the force signal. Therefore, a Kalman filter was applied, which corrects its prediction of the system's state using the available data [33]. After these pre-processing steps, the average forces $F_{i,ave}$ were calculated in each Cartesian direction. The average cutting forces obtained for the different feeds per tooth f_z over the milling length l are depicted in Figure 4. The average forces increase for higher values of f_z with an initial cutting-edge radius of 5 µm (sharp). The cutting force components in x- and z-directions slightly increase with the ascendant milling length. The most significant effect of a change in the microgeometry of the cutting edge over the milling path caused by tool wear can be observed in the cutting force component F_y.

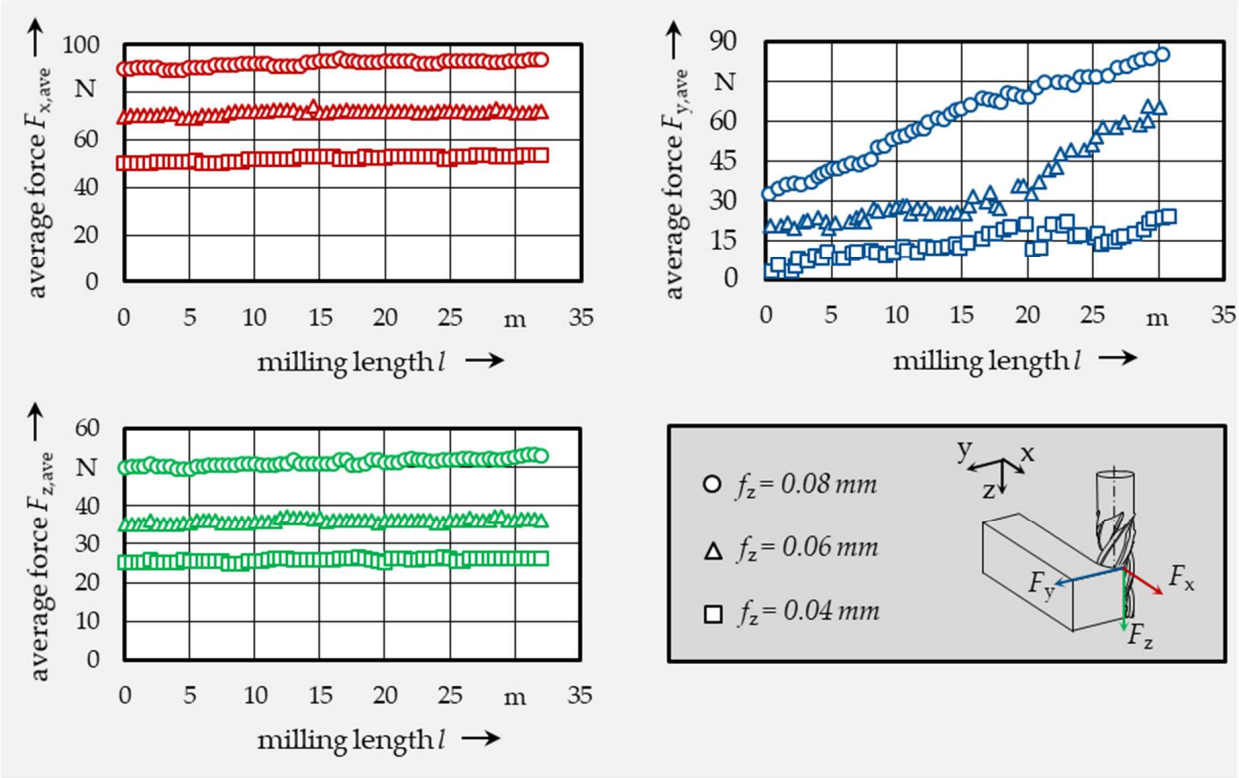

Figure 4. Measured cutting forces in x-, y- and z-directions over the milling length for different feeds per tooth.

4.2. Tool Wear Behavior

The cutting-edge radius is assumed to increase with progressive tool wear and the experiments conducted in this study confirm this trend. The individual cutting edges exhibit a uniform wear behavior (Figure 5). The results show an increase in the cutting-edge radius over the milling length for all three tested feeds per tooth f_z (0.04 mm, 0.06 mm, and 0.08 mm).

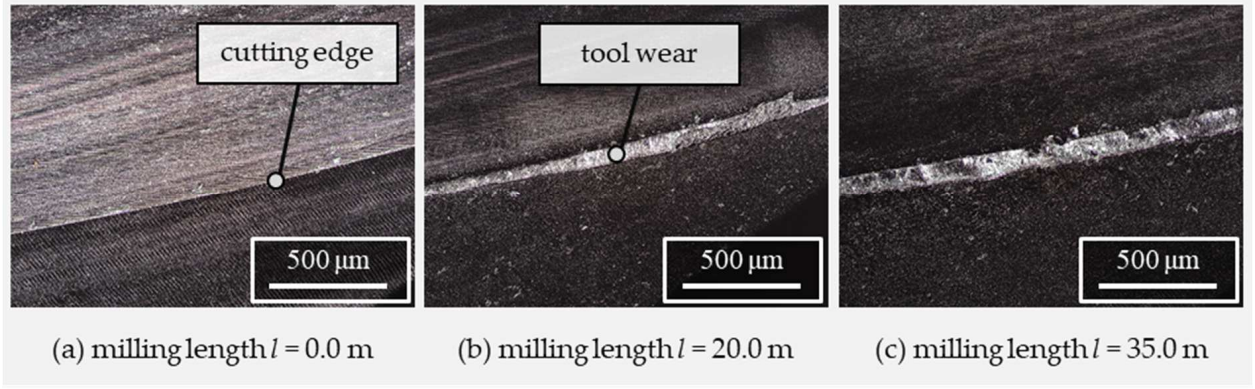

Figure 5. Progressive tool wear for a feed per tooth f_z of 0.06 mm at the cutting edge for different milling lengths l recorded with the KEYENCE VK-X1050 with a magnification of 10×.

Additionally, the experiments revealed that the tools with the same feed per tooth (i.e., Tools 1–3, Tools 4–6, and Tools 7–9) exhibited similar wear behavior. In this case, the change in the cutting-edge rounding was increased by selecting a higher feed per tooth. After a milling length of 35 m, a maximum cutting-edge radius of 31 µm for a feed per tooth of 0.04 mm, 43 µm for 0.06 mm and 54 µm for 0.08 mm was measured. The values for

the measured cutting-edge radius r_β over the milling length l for each of the three feed per tooth values are shown in Figure 6.

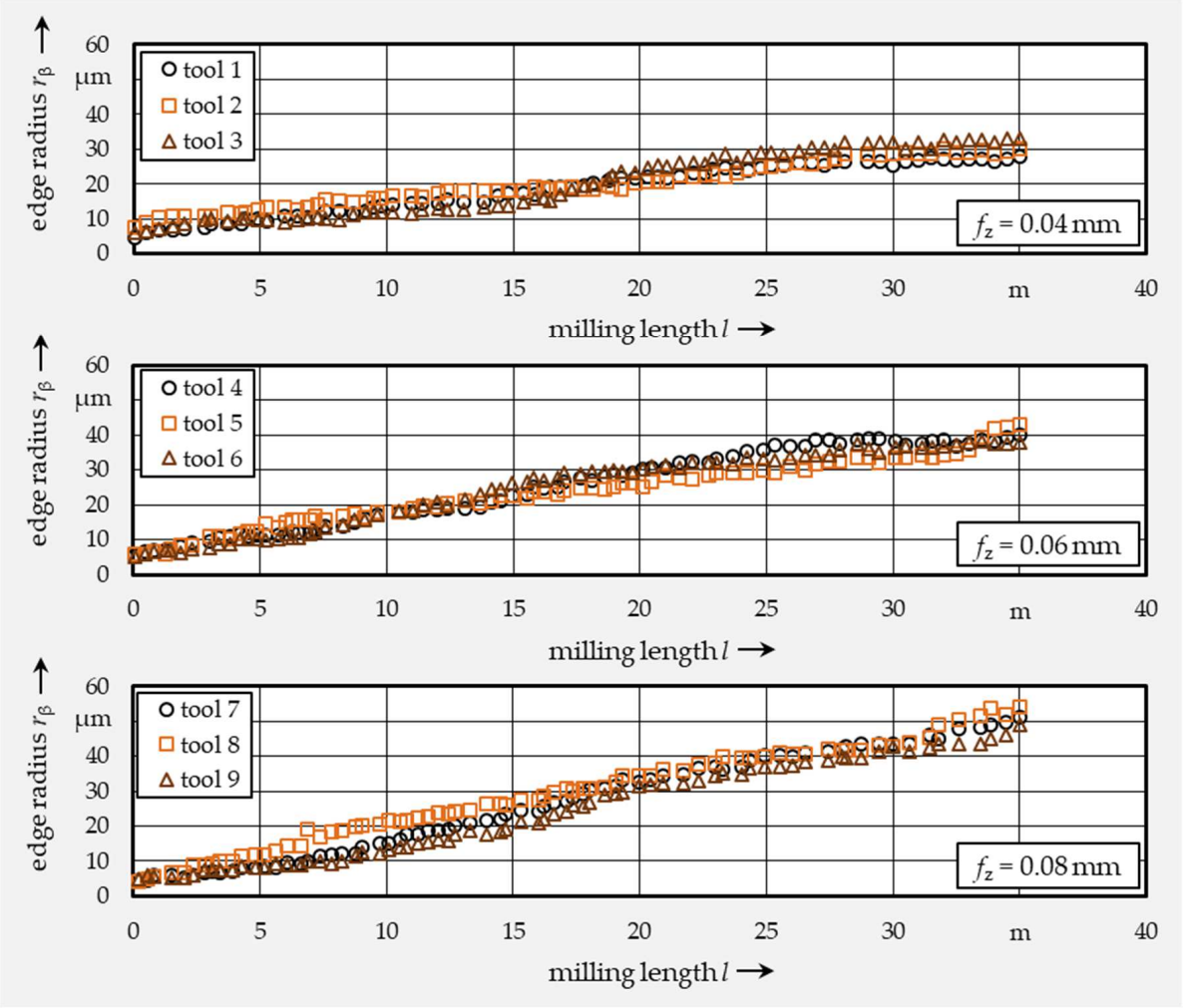

Figure 6. Change in the cutting-edge radius over the milling length.

4.3. Influence of the Edge Radius on the Surface Residual Stress

The results of the residual stress measurements after peripheral milling with defined cutting-edge radii always show compressive residual stresses on the surface of the machined components made of Ti-6Al-4V (Figure 7). The magnitude of the compressive residual stresses perpendicular to the feed direction (Figure 4, z-direction) and in the feed direction (Figure 4, x-direction) increases with higher cutting-edge radii. For a feed per tooth of 0.04 mm, the residual compressive stresses perpendicular to the feed direction showed a change from −114 MPa with a cutting-edge radius of 5 µm (sharp) to −289 MPa for a cutting edge rounding of 60 µm (minus sign indicates compressive stresses). Additionally, the machining-induced residual stresses in the feed direction showed a change from −52 MPa to −253 MPa. A higher feed per tooth reduces the maximum residual compressive stresses on the surface for the same cutting-edge microgeometry. With a feed per tooth of 0.06 mm, maximum residual compressive stresses of −246 MPa perpendicular to the feed direction and −244 MPa in the feed direction were induced in the machined surface with a cutting-edge rounding of 60 µm.

The cutting-edge radius thus significantly affects the resulting residual stresses after peripheral milling of Ti-6Al-4V. Consequently, knowing the cutting-edge rounding, the residual stress state on the surface and in the sub-surface could be derived. However,

the microgeometry of the cutting edge is unknown during the milling process and must therefore be determined.

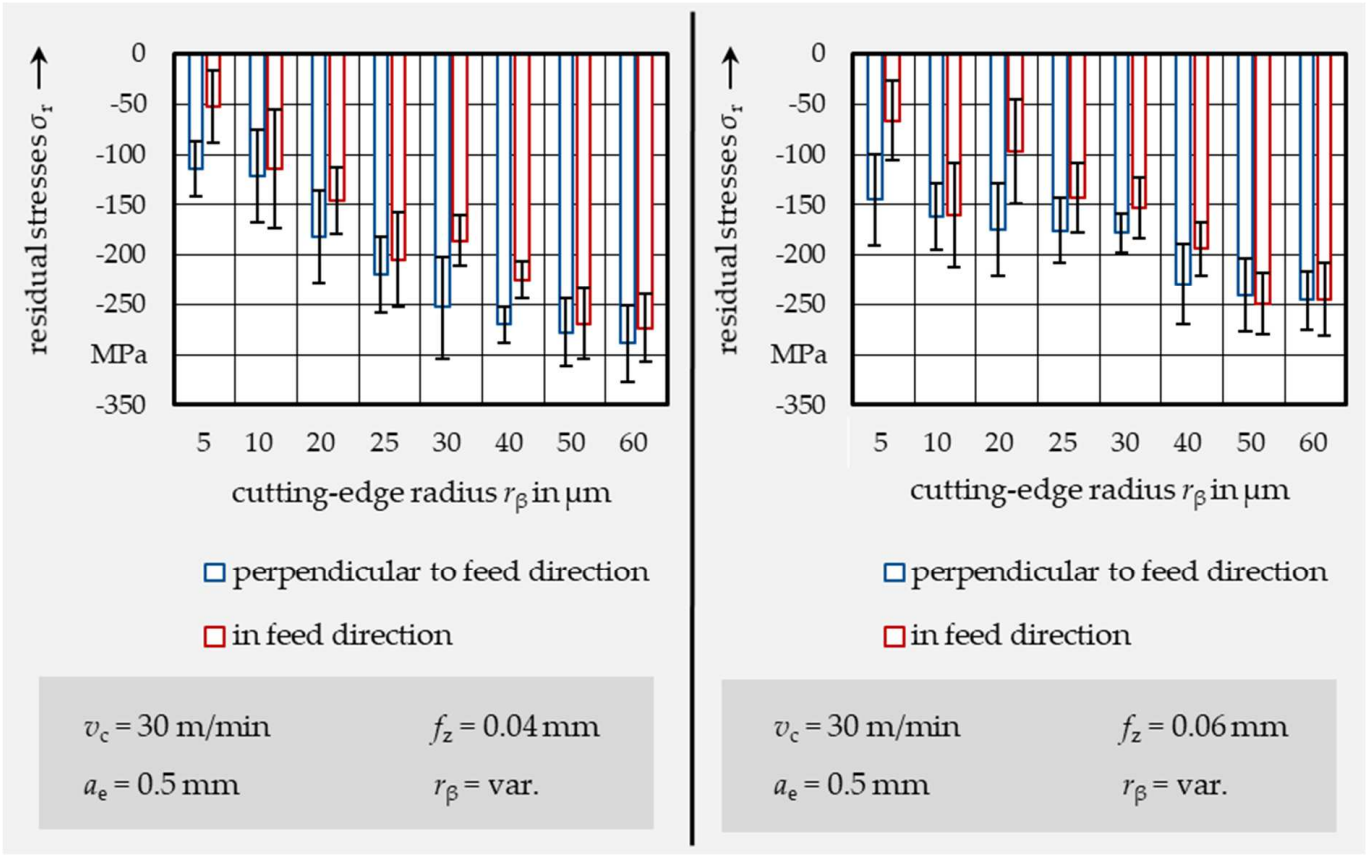

Figure 7. Effect of the cutting-edge radius on the surface residual stresses for two different feeds per tooth f_z.

5. Tool Wear Prediction Model

5.1. Data Acquisition

For determining the cutting-edge radius using ML, a database was first built up which contains

- the process forces in the Cartesian directions (F_x, F_y, and F_z),
- the process parameters (v_c, a_e, and f_z), and
- the current maximum cutting-edge radius (r_β).

For this purpose, the process forces were recorded during the peripheral milling process of Ti-6Al-4V using the sensor tool holder. In addition, the cutting-edge radius was measured offline in defined intervals of 0.5 m. A ML model was trained to accurately predict the cutting-edge radius at any given time during the milling process by building up a database of in-process data and offline cutting-edge radius measurements.

5.2. Signal Processing and Data Analysis

The relevant input data for the tool wear prediction model are the forces in x-, y-, and z-directions and the feed per tooth f_z. These input data must be pre-processed to use them in the tool wear prediction model (Figure 8). For the forces, the mean values were subtracted from the signal. Because the feed values were 0.04 mm, 0.06 mm and 0.08 mm while the measured forces were in a two- to three-digit range, min–max scaling was applied. Thus, the input data were scaled to the interval [0, 1].

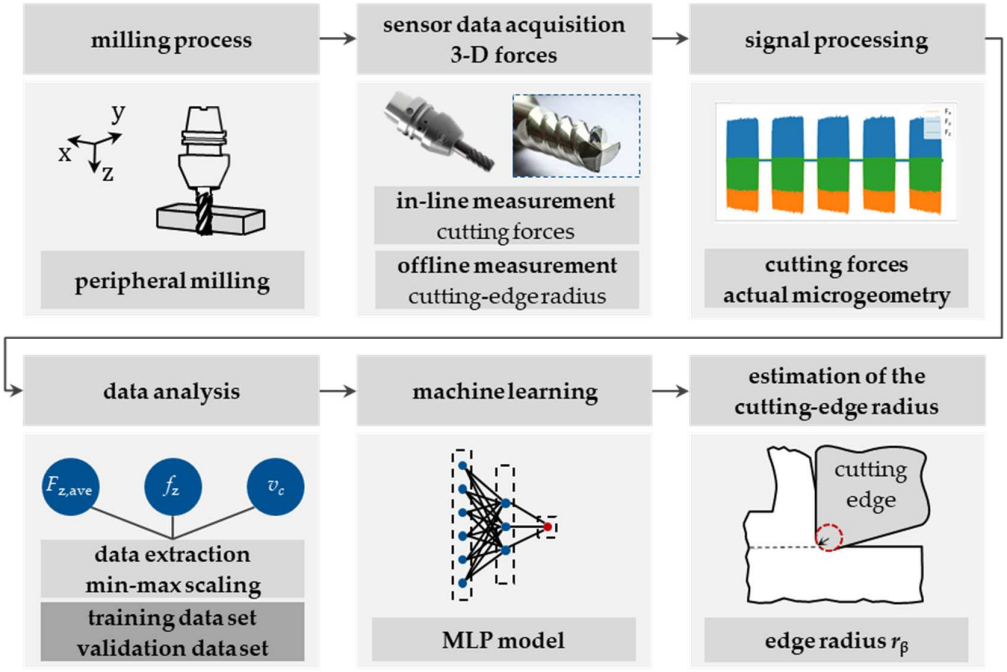

Figure 8. Methodology for determining the cutting-edge radius using an MLP regressor based on the measured cutting forces.

5.3. Machine Learning

After the generation and the pre-processing of the input data, ML algorithms were applied to discover the relationship between the cutting forces F_x, F_y, and F_z and the cutting-edge rounding r_β for the different feeds per tooth f_z. For the data analysis, a universal function approximator in the form of an MLP was applied and the performance of the data set was evaluated. The MLP is a type of artificial neural network (ANN) composed of multiple layers of interconnected neurons. The most common type of MLP consists of a single input layer, one or more hidden layers, and a single output layer. The neurons in each layer are connected to neurons in the previous and following layers with connections. The input layer receives the input data and has several neurons equal to the inputs in the data set. The hidden layers process the data using weights and biases. The output layer has a single neuron and produces the final result. An MLP has a fully connected architecture. This denotes that each of the neurons in one layer is connected to every neuron in the following layer [34].

The given problem is one of regression in the supervised learning case because the data points are labeled with an actual number, the current cutting-edge radius. MLPs are commonly used for supervised learning tasks. They are also known as feedforward neural networks, as the data flows through the network in only one direction, from input to output. The limited memory BFGS (L-BFGS) algorithm from the family of Quasi-Newton solvers was applied next. Solvers are one of the hyperparameters of an ANN. A solver is an algorithm used in the backpropagation process to calculate the weights of the neural network. For performance and flexibility concerning the solver implementations provided, a sklearn.neural_network.MLP regressor class was used. This class provides the L-BFGS algorithm [25].

The MLP regressor uses activation functions to introduce non-linearity into the prediction model. The activation function is a function that maps the input of the neuron onto its output [35]. Basic activation functions are commonly designed to keep the signal within a wanted range (tanh), or to eliminate unwanted elements (ReLU). To predict the cutting-edge radius based on the cutting forces and the process parameters, the tanh function and the ReLU function were compared. To optimize the model architecture, several hyperparameters were varied, such as the number of layers, the number of neurons in each layer,

the learning rate, and the used activation function. Additionally, the maximum number of gradient steps was considered a hyperparameter, which was increased by steps of 50 within a range of [50, 300]. The learning rate α was chosen to be 0.001, which was defined as the default setting. To generate a training and validation data set, an 80:20 split was applied. To preselect all possible parameter combinations, test runs of the prediction were performed. Due to the prevalence of the maximum root mean square error (RMSE) of 15.97 µm, a threshold value of 16 µm was set. The methodology for determining the cutting-edge radius using an MLP regressor based on the measured cutting forces is illustrated in Figure 8.

6. Modeling Results

The predicted cutting-edge radii were compared with the measured radii of the data set to evaluate the performance of the tool wear prediction model. The RMSE was calculated to assess the prediction results. The number of gradient steps that led to minor errors was the minimum limit of the tested range, i.e., 50. An RMSE of 15.76 µm was obtained. The range was therefore decreased, and the limits were lowered to values ranging from 10 to 50 in increments of 5. The errors decreased for the lower number of allowed gradient steps. The produced errors for the different architectures using the L-BFGS solver with the ReLU function are shown in Table 3. The prediction model using the ReLU function as an activation function consisting of three hidden layers with four hidden neurons each achieved an error of 13.23 µm for a learning rate α of 0.00868 and 20 gradient steps.

Table 3. RMSE for different architectures using L-BFGS with ReLU activation.

Activ. Function	Hidden Layers	Hidden Neurons	Max. Gradient Steps	RMSE
ReLU	2	3	50	15.76 µm
ReLU	3	4	50	15.40 µm
ReLU	1	4	10	13.75 µm
ReLU	3	4	20	13.23 µm

Using the tanh activation function (Table 4), a non-linear dependency between r_β and F_y was found. As the dependency between r_β and F_y was the most remarkable (see Figure 4), an MLP model was built using $F_{y,norm}$ as the only input. The result was an RMSE of 15.56 µm for four hidden layers with four hidden neurons and 50 gradient steps. By reducing the maximum gradient steps, the RMSE could be lowered. In addition, the number of hidden layers and hidden neurons was changed. Using the normalized force $F_{y,norm}$ as input, the lowest error was 8.94 µm for four hidden layers including three hidden neurons each and a number of 25 maximum gradient steps.

Table 4. RMSE for different architectures using L-BFGS with tanh activation.

Activ. Function	Hidden Layers	Hidden Neurons	Max. Gradient Steps	RMSE
tanh	4	4	50	15.56 µm
tanh	1	4	25	14.16 µm
tanh	4	2	20	13.99 µm
tanh	4	3	35	9.00 µm
tanh	3	3	35	8.98 µm
tanh	3	3	30	8.97 µm
tanh	4	3	25	8.94 µm

The predicted values of the cutting-edge roundings $r_{\beta,pred}$ that were generated using the elaborated model were plotted against the measured cutting-edge radii $r_{\beta,true}$. The corresponding graph is shown in Figure 9. The results for evaluating this model on the complete data set are promising.

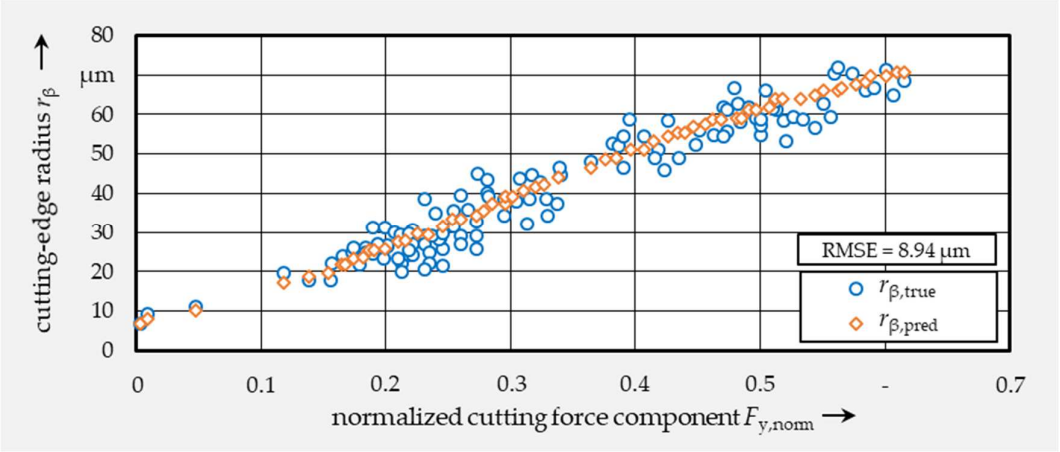

Figure 9. Predicted cutting-edge radii $r_{\beta,pred}$ vs. true response $r_{\beta,true}$ for an MLP with L-BFGS solver, a learning rate α of 0.001, tanh activation function, four hidden layers with three neurons and 25 gradient steps based on the normalized cutting force component $F_{y,norm}$.

7. Conclusions

The aim of this work was the determination of the current maximum cutting-edge radius based on the cutting forces during peripheral milling using Machine Learning. The investigations presented in this publication concern the change in the cutting-edge radius due to tool wear during peripheral milling of the titanium alloy Ti-6Al-4V. Experiments using different feeds per tooth were performed. The cutting forces were measured using a sensor tool holder during the milling tests. The cutting-edge radius was measured offline at regular intervals using a laser scanning microscope. In addition, tests were performed with prepared cutting-edge radii with subsequent measurements of the residual stresses on the machined surface. The main findings of the analysis of the experimental studies are as follows:

- The forces in x-, y- and z-directions increased over the milling length. In particular, an increase in the forces in the y-direction F_y was observed.
- An increase in the cutting-edge rounding over the milling length could be observed. Due to abrasive tool wear, material was removed from the cutting edges.
- Residual stresses were consistently obtained within the compression range. A change in the cutting-edge radii from 5 µm to 60 µm led to a significant increase in the residual compressive stresses.

The machining-induced residual stresses after the peripheral milling process strongly depend on the actual cutting-edge geometry. The radius of the cutting edges cannot be measured directly during machining and must therefore be determined based on a model.

To determine the microgeometry of the cutting edges during the milling process, the relationship between the size of the cutting-edge radius and the resulting cutting forces during the milling process was used to generate a database. A training and a validation data set was built through signal processing and data analysis. Finally, the MLP method was applied using different architectures. The performance of the algorithm was measured with the RMSE. The best results were achieved for an MLP with an L-BFGS solver with a tanh activation function. In conclusion, the developed tool wear prediction model performed well on the data set. The forces are suitable for predicting the cutting-edge radius, especially the force component in the y-direction.

Overall, the experiments and the developed prediction model provide insights into the effect of changing edge microgeometry due to tool wear on the cutting forces and the resulting residual stresses during the peripheral milling of Ti-6Al-4V. During the machining process, the state of residual stresses in the sub-surface of the workpiece is influenced by the choice of the process parameters and the micro-geometry of the cutting edge. The most important parameter for the residual stresses induced by machining is

the cutting-edge radius. This significant factor makes a difference in the cutting behavior in advanced manufacturing, covering the occurring mechanical loads and the machining-induced surface integrity. A change in the cutting-edge radius due to tool wear induces higher compressive residual stresses, which have a positive effect on the service life of the component. These observations could be correlated with higher ploughing forces. When milling Ti-6Al-4V, this factor influences the residual stress state due to peripheral milling. The predicted cutting-edge radii can be used in future work as an input variable for the model-based determination of the residual stress state, depending on the cutting-edge geometry. In addition, further work should investigate the influence of tool wear on other surface integrity properties, such as surface roughness and hardness.

Author Contributions: Conceptualization, M.W.; methodology, M.W.; software, M.W.; validation, M.W.; formal analysis, M.W.; investigation, M.W.; resources, M.W.; data curation, M.W.; writing—original draft preparation, M.W.; writing—review and editing, M.W., M.F.Z. and R.H.; visualization, M.W.; supervision, M.F.Z. and M.W.; project administration, M.W.; funding acquisition, M.F.Z. All authors have read and agreed to the published version of the manuscript.

Funding: This research was funded by the German Research Foundation (DFG) in the priority program SPP 2086, grant numbers ZA 288/72-1, project number 359102403.

Data Availability Statement: The reference data presented in this study are available upon request from the corresponding author.

Conflicts of Interest: The authors declare that they have no conflict of interest.

References

1. Ulutan, D.; Ozel, T. Machining induced surface integrity in titanium and nickel alloys: A review. *Int. J. Mach. Tools Manuf.* **2011**, *51*, 250–280. [CrossRef]
2. Niknam, S.A.; Khettabi, R.; Songmene, V. Erratum to: Machinability and Machining of Titanium Alloys: A Review. In *Machining of Titanium Alloys*; Davim, J.P., Ed.; Springer: Berlin/Heidelberg, Germany, 2014; pp. 1–30. ISBN 978-3-662-43901-2.
3. Sridhar, B.; Devananda, G.; Ramachandra, K.; Bhat, R. Effect of machining parameters and heat treatment on the residual stress distribution in titanium alloy IMI-834. *J. Mater. Process. Technol.* **2003**, *139*, 628–634. [CrossRef]
4. Che-Haron, C. Tool life and surface integrity in turning titanium alloy. *J. Mater. Process. Technol.* **2001**, *118*, 231–237. [CrossRef]
5. Wimmer, M.; Woelfle, C.; Krempaszky, C.; Zaeh, M. The influences of process parameters on the thermo-mechanical workpiece load and the sub-surface residual stresses during peripheral milling of Ti-6Al-4V. *Procedia CIRP* **2021**, *102*, 471–476. [CrossRef]
6. Zhang, P.; Liu, Z. Effect of sequential turning and burnishing on the surface integrity of Cr–Ni-based stainless steel formed by laser cladding process. *Surf. Coatings Technol.* **2015**, *276*, 327–335. [CrossRef]
7. Yang, D.; Xiao, X.; Liu, Y.; Sun, J. Peripheral milling-induced residual stress and its effect on tensile–tensile fatigue life of aeronautic titanium alloy Ti–6Al–4V. *Aeronaut. J.* **2019**, *123*, 212–229. [CrossRef]
8. Schoop, J.; Hasan, M.; Zannoun, H. Physics-Informed and Data-Driven Prediction of Residual Stress in Three-Dimensional Machining. *Exp. Mech.* **2022**, *62*, 1461–1474. [CrossRef]
9. Schoop, J. In-Situ Calibrated Modeling of Residual Stresses Induced in Machining under Various Cooling and Lubricating Environments. *Lubricants* **2021**, *9*, 28. [CrossRef]
10. Li, X.; Wang, Z.; Yang, S.; Guo, Z.; Zhou, Y.; Han, K. Influence of turning tool wear on the surface integrity and anti-fatigue behavior of Ti1023. *Adv. Mech. Eng.* **2021**, *13*, 16878140211011278. [CrossRef]
11. Denkena, B.; Grove, T.; Maiss, O. Influence of the cutting-edge radius on surface integrity in hard turning of roller bearing inner rings. *Prod. Eng. Res. Devel.* **2015**, *9*, 299–305. [CrossRef]
12. Li, B.; Zhang, S.; Yan, Z.; Jiang, D. Influence of edge hone radius on cutting forces, surface integrity, and surface oxidation in hard milling of AISI H13 steel. *Int. J. Adv. Manuf. Technol.* **2018**, *95*, 1153–1164. [CrossRef]
13. Nespor, D. Randzonenbeeinflussung durch die Rekonturierung Komplexer Investitionsgüter aus Ti-6Al-4V. Ph.D. Thesis, Leibniz Universität Hannover, Hannover, Germany, 2015.
14. Wyen, C.-F.; Jaeger, D.; Wegener, K. Influence of cutting-edge radius on surface integrity and burr formation in milling titanium. *Int. J. Adv. Manuf. Technol.* **2013**, *67*, 589–599. [CrossRef]
15. Coelho, R.; Silva, L.; Braghini, A.; Bezerra, A. Some effects of cutting-edge preparation and geometric modifications when turning INCONEL 718™ at high cutting speeds. *J. Mater. Process. Technol.* **2004**, *148*, 147–153. [CrossRef]
16. Özel, T.; Ulutan, D. Prediction of machining induced residual stresses in turning of titanium and nickel-based alloys with experiments and finite element simulations. *CIRP Ann.* **2012**, *61*, 547–550. [CrossRef]
17. Wyen, C.-F.; Wegener, K. Influence of cutting-edge radius on cutting forces in machining titanium. *CIRP Ann.* **2010**, *59*, 93–96. [CrossRef]

18. Albrecht, P. New Developments in the Theory of the Metal-Cutting Process: Part I. The Ploughing Process in Metal Cutting. *J. Eng. Ind.* **1960**, *82*, 348–357. [CrossRef]
19. *DIN 6580-10*; Begriffe Der Zerspantechnik; Bewegungen und Geometrie des Zerspanvorganges. Beuth Verlag GmbH.: Berlin, Germany, 1985.
20. *DIN 6584*; Begriffe Der Zerspantechnik; Kräfte, Energie, Arbeit, Leistungen. Beuth Verlag GmbH.: Berlin, Germany, 1982.
21. Merchant, M.E. Mechanics of the Metal Cutting Process. I. Orthogonal Cutting and a Type 2 Chip. *J. Appl. Phys.* **1945**, *16*, 267–275. [CrossRef]
22. Altintas, Y. *Manufacturing Automation: Metal Cutting Mechanics, Machine Tool Vibrations, and Cnc Design*, 2nd ed.; Cambridge University Press: New York, NY, USA, 2012; ISBN 9781107001480.
23. Moufki, A.; Dudzinski, D.; Le Coz, G. Prediction of cutting forces from an analytical model of oblique cutting, application to peripheral milling of Ti-6Al-4V alloy. *Int. J. Adv. Manuf. Technol.* **2015**, *81*, 615–626. [CrossRef]
24. Lv, D.; Wang, Y.; Yu, X. Effects of cutting-edge radius on cutting force, tool wear, and life in milling of SUS-316L steel. *Int. J. Adv. Manuf. Technol.* **2020**, *111*, 2833–2844. [CrossRef]
25. Murphy, K.P. *Machine Learning: A Probabilistic Perspective*; MIT Press: Cambridge, MA, USA, 2012; ISBN 9780262305242.
26. Bishop, C.M. *Pattern Recognition and Machine Learning*; Springer: New York, NY, USA, 2006; ISBN 0387310738.
27. Wimmer, M.; Hameed, M.Z.S.; Wölfle, C.; Weisbrodt, V.; Zaeh, M.F.; Werner, E.; Krempaszky, C.; Semm, T. The influence of the process parameters on the surface integrity during peripheral milling of Ti-6Al-4V. *TM-Tech. Mess.* **2020**, *87*, 721–731. [CrossRef]
28. *DIN 6581*; Bezugssysteme und Winkel am Schneidteil des Werkzeuges. German Institute for Standardization: Berlin, Germany, 1985.
29. *ISO 3002-1*; Basic Quantities in Cutting and Grinding; General Terms, Reference Systems, Tool and Working Angles, Chip Breakers. 1st ed. International Organization for Standardization: Geneva, Switzerland, 1982.
30. Wyen, C.-F.; Knapp, W.; Wegener, K. A new method for the characterization of rounded cutting edges. *Int. J. Adv. Manuf. Technol.* **2012**, *59*, 899–914. [CrossRef]
31. Eigenmann, B.; Macherauch, E. Röntgenographische Untersuchung von Spannungszuständen in Werkstoffen. Teil III. Fortsetzung von Matwiss. und Werkstofftechn. 3/1995, 148–160 and 4/1995, 199–216. *Materialwiss. Werkst.* **1995**, *27*, 426–437. [CrossRef]
32. X-ray Diffraction Residual-Stress Techniques. In *X-ray Diffraction Residual Stress Techniques In: Metals handbook*; American Society for Metals (Ed.) ASM International: Metals Park, OH, USA, 1986; pp. 440–458. ISBN 978-1-62708-213-6.
33. Chui, C.K.; Chen, G. (Eds.) *Kalman Filtering*, 5th ed.; Springer International Publishing: Cham, Switzerland, 2017; ISBN 978-3-319-47610-0.
34. Hastie, T.; Tibshirani, R.; Friedman, J. *The Elements of Statistical Learning: Data Mining, Inference, and Prediction*, 2nd ed.; Springer Series in Statistics; Springer: New York, NY, USA, 2009; ISBN 978-0-387-84857-0.
35. Goodfellow, I.; Bengio, Y.; Courville, A. *Deep Learning*; MIT Press: Cambridge, MA, USA, 2016; ISBN 0-262-33737-1.